The VLT-FLAMES survey of massive stars: NGC 346-013 as a test case for massive close binary evolution[⋆]

B. W. Ritchie[1,2], V. E. Stroud[1,3,4], C. J. Evans[5], J. S. Clark[1], I. Hunter[6], D. J. Lennon[7], N. Langer[8,9], and S. J. Smartt[6]

[1] Department of Physics and Astronomy, The Open University, Walton Hall, Milton Keynes MK7 6AA, UK
  e-mail: b.ritchie@open.ac.uk
[2] Lockheed Martin Integrated Systems, Building 1500, Langstone, Hampshire, PO9 1SA, UK
[3] Faulkes Telescope Project, School of Physics and Astronomy, Cardiff University, Cardiff, CF24 3AA, UK
[4] Division of Earth, Space and Environment, University of Glamorgan, Pontypridd, CF37 1DL, UK
[5] UK Astronomy Technology Centre, Royal Observatory Edinburgh, Blackford Hill, Edinburgh, EH9 3HJ, UK
[6] Department of Physics & Astronomy, Queen's University Belfast, Belfast BT7 1NN, Northern Ireland, UK
[7] ESA/STScI, 3700 San Martin Drive, Baltimore, MD 21218, USA
[8] Argelander-Institut für Astronomie der Universität Bonn, Auf dem Hügel 71, 53121 Bonn, Germany
[9] Astronomical Institute, Utrecht University, Princetonplein 5, Utrecht, The Netherlands

ABSTRACT

Context. NGC 346-013 is a peculiar double-lined eclipsing binary in the Small Magellanic Cloud (SMC) discovered by the VLT-FLAMES survey of massive stars.
Aims. We use spectroscopic and photometric observations to investigate the physical properties and evolutionary history of NGC 346-013.
Methods. Spectra obtained with VLT/FLAMES are used to construct a radial velocity curve for NGC 346-013 and to characterise the early B-type secondary. Photometry obtained with the Faulkes Telescope South is then used to derive orbital parameters, while spectra of the secondary are compared with synthetic spectra from TLUSTY model atmospheres.
Results. The orbital period is found to be 4.20381(12) days, with masses of 19.1 ± 1.0 and 11.9 ± 0.6 $M_{\odot}$. The primary is a rapidly rotating ($v_{\rm rot} = 320 \pm 30$ km s^{-1}) late-O dwarf while the secondary, an early-B giant, displays near-synchronous rotation and has filled its Roche lobe, implying that it was originally the more massive component with recent mass transfer "spinning up" the primary to near-critical rotation. Comparison with synthetic spectra finds temperatures of 34.5 kK and 24.5 kK for the primary and secondary respectively, with the nitrogen abundance of the secondary enhanced compared to baseline values for the SMC, consistent with the predictions of models of interacting binaries.
Conclusions. NGC 346-013 likely evolved via non-conservative mass transfer in a system with initial masses ~22+15 $M_{\odot}$, with the well-constrained orbital solution and atmospheric parameters making it an excellent candidate for tailored modelling with binary evolution codes. This system will form a cornerstone in constraining the physics of thermal timescale mass transfer, and the associated mass transfer efficiency, in massive close binary systems.

Key words. stars: early-type – stars: fundamental parameters – binaries: spectroscopic – Magellanic Clouds

1. Introduction

Binary systems are of critical importance for understanding the formation and evolution of massive stars. They permit both the direct determination of fundamental stellar properties such as mass and radius, and, through properties such as orbital period, eccentricity and mass ratio, offer insight into the processes of massive star formation and dynamical interactions in the natal cluster. Binarity will strongly influence the evolutionary path both components will follow, with tidal interaction affecting rotational mixing (de Mink et al. 2009) and transfer of mass and angular momentum in the later evolutionary stages leading to a distribution of spectral types that differs significantly from single-star population models (Eldridge et al. 2008). Ejection of the primary's hydrogen mantle during close binary evolution will shape both the type of supernova and the nature of the

subsequent relativistic object (Wellstein & Langer 1999; Brown et al. 2001), while massive secondaries spun-up to critical rotation during mass transfer represent candidates for γ-ray burst progenitors (Woosley & Heger 2006; Cantiello et al. 2007). Properties derived from massive binary systems may also provide key constraints on the formation and evolution of wider stellar populations (Ritchie et al. 2010; Clark et al. 2011).

In this paper, we examine the short-period eclipsing binary NGC 346-013[1] discovered in the VLT-FLAMES survey of massive stars[2] field centred on NGC 346, a young, massive cluster located at the centre of N66 (Henize 1956), the largest H II region in the Small Magellanic Cloud (SMC). The region has undergone extensive star formation in recent times, with NGC 346 hosting the largest population of O-type stars in the

---

[1] RA = 00:59:30.27, δ = −72 : 09 : 09.3 (J2000); star #782 from Massey et al. (1989), who list m_v = 14.46, $(B - V) = -0.18$, and a reddening-free colour index $Q = (U - B) - 0.72(B - V) = -0.79$.
[2] Evans et al. (2005, 2006).

SMC (Massey et al. 1989; Walborn et al. 2000; Evans et al. 2006), while a large population of massive young stellar objects (YSOs) indicate that star formation is ongoing (Simon et al. 2007; Gouliermis et al. 2010). Studies of pre-main sequence stars indicate a complex history, with major star formation in NGC 346 starting ~6 Myr ago and lasting about 3 Myr, while an older population indicates an earlier epoch of star formation that took place ~10 Myr ago (Hennekemper et al. 2008; Cignoni et al. 2010, 2011).

The main morphological features seen in the FLAMES spectra of NGC 346-013 were summarized by Evans et al. (2006), who noted lines of He I, C III, N III and Si III consistent with a spectral type of B1–1.5 and velocity shifts between spectra that spanned ~400 km s^{-1}. However, a broad He II λ4686 absorption line was observed moving in the opposite sense to the other features, indicating the presence of a companion with an earlier spectral type, with the lower amplitude of the line indicating that it traces the more massive object in the system: throughout this paper we refer to the hotter, more massive object as the primary and the B-type star as the secondary, acknowledging the problems in applying these terms to evolved, short-period binary systems in which mass exchange may confuse their conventional meaning.

The peculiar hot, underluminous primary and the presence of an apparently rotationally-broadened He II line suggest that NGC 346-013 is seen in a brief evolutionary phase shortly after the end of thermal-timescale Roche-lobe overflow, where mass transfer has reversed the initial mass ratio of the system and "spun-up" the mass-gainer to rapid rotation. Such a system is of critical importance to understanding the efficiency of mass transfer in short-period binaries (Wellstein & Langer 1999; Wellstein et al. 2001; Petrovic et al. 2005; de Mink et al. 2007), a process that shapes both the ongoing evolution of the systems and the extreme evolutionary endpoints that can only be reached via extensive binary interaction, such as Wray 977 (a ~40+1.4 $M_\odot$ B1 Ia$^+$/neutron star binary; Wellstein & Langer 1999; Kaper et al. 2006), 4U1700-37 (a 58+2.4 $M_\odot$ O6.5 Iaf$^+$/compact object binary; Clark et al. 2002) or the magnetar CXOU J164710.2-455216, which formed a neutron star despite a minimum progenitor mass approaching 50 $M_\odot$ (Ritchie et al. 2010). We have therefore undertaken a programme of observations aimed at deriving accurate properties for the two components of NGC 346-013, supplementing the original dataset discussed by Evans et al. (2006) with an additional 14 spectra obtained with FLAMES in 2008 and a photometric dataset acquired during 2008–2009 with the Faulkes Telescope South (FTS). Details of our observations are given in Sect. 2, while in Sect. 3 we use TLUSTY model atmospheres (e.g. Hubeny & Lanz 1995) to estimate the temperature, gravity, rotational velocity and chemical abundances of the early-B secondary that dominates the FLAMES spectra. In Sect. 4 we derive orbital parameters from the radial velocity (RV) and photometric datasets, and discuss the evolution of NGC 346-013 and implications for NGC 346 in Sect. 5.

2. Observational details

2.1. Spectroscopy

A total of 32 spectra of NGC 346-013 were obtained in 2006 as part of the VLT-FLAMES survey of massive stars field centred on NGC 346 (Evans et al. 2006). Observations were taken with the GIRAFFE spectrograph, with the five relevant wavelength

Table 1. FLAMES setups and lines used for RV measurement.

Setup	Coverage (Å)	$R(\lambda_c)$	Lines
HR02	3854–4049	19 600	He I λ4009, He I λ4026
HR03	4033–4201	24 800	He I λ4121, He I λ4144
HR04	4188–4392	20 350	–
HR05	4340–4587	18 470	He I λ4388, He I λ4471
			Si III $\lambda\lambda$4553, 4568
HR06	4538–4759	20 350	Si III $\lambda\lambda$4553, 4568
			N III λ4642, C III λ4650
			He II λ4686, He I λ4713

settings used listed in Table 1[3]. An integration time of 2275 s was used, with the exception of HR06 #08 (MJD = 52 988.18332) which used an integration time of 2500 s (related to execution of the service mode observations). The data were reduced using version 1.10 of the Giraffe Base-Line Reduction Software (girBLDRS; Blecha et al. 2003), with sky spectra subtracted from each target using the *Starlink* package DIPSO (Howarth et al. 2003). A further 14 spectra in HR02 mode were obtained during a 9-day period in July 2008 as part of a programme of follow-up observations of the cluster (PI: Hunter), each with an integration time of 2662 s. These data were pipeline reduced using version 3.6.8 of ESOREX[4], with individual spectra shifted to the heliocentric frame using the IRAF[5] RVCORRECT and DOPCOR routines. A median sky spectrum was then created from the sky fibres and subtracted from each object spectrum. The signal-to-noise ratio was in excess of ~75, varying slightly depending on the exact conditions when individual observations were obtained.

The strong Balmer-series lines could not be used for RV measurement due to their broad wings, lack of sharp core, and presence of nebular emission, and RVs were instead measured using the strongest available helium and (when present) metal absorption lines in each spectrum: the lines used for each setup are listed in Table 1. The He I lines appear to show only minimal nebular components, but are notably asymmetric in most spectra with a strong, narrow and symmetric core arising in the secondary and a weaker contribution from the hotter primary in the wings; example profiles near maximum separation are shown in Fig. 1. RVs for the secondary were therefore measured by fitting profiles to just the core of the strong He I component, with the derived RVs in excellent agreement with other lines of C III and Si III that appear free from strong contamination by the primary. The derived RV for each spectrum is then an error-weighted average of individual absorption lines. Unblended lines from the primary are only directly visible in the HR06 data, with a comparison of spectra from 2003 October 14 and 2003 December 15 (MJDs of 52 926 and 52 988 respectively) clearly showing the antiphase motion of the He II λ4686 line (see Fig. 4 of Evans et al. 2006), while the weakness of the corresponding He II λ4542 absorption line suggests a classifi-

---

[3] A further setting, HR14A (covering 6391–6701 Å) is described by Evans et al. (2006) but is not used here, as Hα and He I λ6678 are strongly blended with nebular emission. Observations in HR04 mode were not used for RV measurement due to a lack of strong metal lines in this region of the spectrum, but the Hδ line was used for surface gravity fits, as discussed in Sect. 3.1.

[4] http://www.eso.org/sci/data-processing/software/cpl/esorex.html

[5] IRAF is distributed by the National Optical Astronomy Observatories, which are operated by the Association of Universities for Research in Astronomy, Inc., under cooperative agreement with the National Science Foundation.

Table 2. Journal of observations.

MJD[a]	Phase[b]	GIRAFFE Setup	RV_{sec} (km s^{-1})	RV_{pri} (km s^{-1})
52 926.08623	0.445	HR06	245 ± 7	
52 926.13820	0.457	HR06	244 ± 20	152 ± 16
52 926.16522	0.464	HR06	226 ± 10	144 ± 15
52 926.20344	0.473	HR06	211 ± 13	111 ± 17
52 926.23039	0.479	HR06	201 ± 5	144 ± 16
52 954.13589	0.117	HR02	313 ± 7	47 ± 6[c]
52 954.16291	0.124	HR02	335 ± 9	
52 954.18986	0.130	HR02	344 ± 10	47 ± 7[c]
52 955.08957	0.344	HR02	370 ± 9	
52 955.11657	0.351	HR02	348 ± 27	40 ± 9[c]
52 955.14352	0.357	HR02	337 ± 14	
52 978.11549	0.822	HR05	−59 ± 5	290 ± 7[c]
52 978.14244	0.828	HR05	−59 ± 12	275 ± 7[c]
52 978.16940	0.835	HR05	−46 ± 14	266 ± 6[c]
52 981.04545	0.519	HR03	139 ± 5	
52 981.07248	0.525	HR03	116 ± 8	
52 981.09943	0.532	HR03	96 ± 5	
52 981.13275	0.539	HR03	91 ± 10	
52 981.15970	0.546	HR03	69 ± 11	
52 981.18665	0.552	HR03	70 ± 5	
52 988.11104	0.199	HR06	396 ± 17	−10 ± 11
52 988.15506	0.210	HR06	412 ± 13	−10 ± 13
52 988.18332	0.217	HR06	406 ± 15	−15 ± 12
53 006.04733	0.466	HR05	226 ± 5	
53 006.07434	0.473	HR05	194 ± 8	
53 006.10131	0.479	HR05	202 ± 15	
54 663.31918	0.693	HR02	−76 ± 5	293 ± 9[c]
54 663.35111	0.701	HR02	−78 ± 6	304 ± 11[c]
54 664.29465	0.925	HR02	64 ± 5	
54 664.32772	0.933	HR02	62 ± 5	
54 665.29193	0.163	HR02	378 ± 5	−2 ± 7[c]
54 666.25561	0.392	HR02	326 ± 6	
54 666.28778	0.400	HR02	294 ± 5	
54 666.35881	0.416	HR02	286 ± 5	
54 666.39125	0.424	HR02	266 ± 5	
54 669.36147	0.131	HR02	342 ± 13	28 ± 8[c]
54 669.39421	0.138	HR02	356 ± 10	
54 670.28291	0.350	HR02	391 ± 9	
54 671.26508	0.584	HR02	42 ± 8	
54 672.28464	0.826	HR02	−66 ± 9	294 ± 9[c]

Notes. [a] MJD given at the midpoint of the integration; [b] or superior conjunction at MJD 52 924.21553(66) and orbital period 4.20381(12) days (see Sect. 4.1); [c] From two-component Gaussian fits to the He I lines.

cation around O9–9.5. However, the HR06 spectra sample only a small portion of the orbit ($\phi \sim$ 0–0.25), and we therefore use two-component Gaussian fits to the the strong He I λ4026 and He I λ4471 lines in the HR02 and HR05 spectra taken near maximum separation to further constrain the amplitude of the primary. The He I profiles are clearly double at these epochs, and satisfactory fits to co-added spectra can be achieved[6]. A full list of derived RVs for both primary and secondary are listed in Table 2.

2.2. Photometry

Photometry was obtained with the Faulkes Telescope South (FTS) 2 m Ritchey-Chrétien Cassegrain, located in Siding Spring, Australia, as part of a follow-up photometric programme

_{──────────}
[6] However, in a number of spectra sky residuals fall within the weak primary component of the He I line, precluding accurate deconvolution despite the primary and secondary being well separated; these spectra are not used in the analysis.
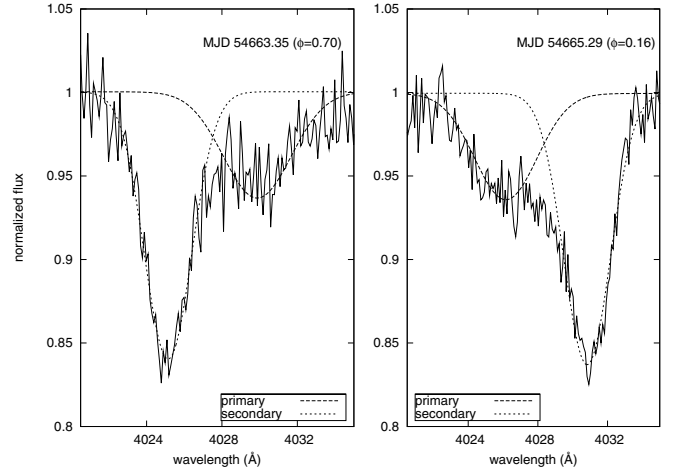

Fig. 1. Two-component Gaussian fit to the He I λ4026 lines near maximum separation at MJD 54 663.35 ($\phi = 0.70$; *left panel*) and approximately half an orbit later at MJD 54 665.29 ($\phi = 0.16$; *right panel*).

to monitor the target clusters of the FLAMES survey. FTS currently uses a Merope camera (EM03), although prior to 2009 January the camera used was an Apogee "Hawkcam" (EA02). Both cameras were coupled with an EV2 CCD42-40DD CCD giving a 4.7′ × 4.7′ field of view and producing images of 2048 × 2048 pixels, binned 2 × 2 to give 1024 × 1024 pixels at 0.278″ pixel^{-1}. The source was observed using a Bessel V filter, with 100 s exposures. Science images were produced using the Faulkes automatic pipeline, which de-biases and flat-fields the raw images.

A total of 104 observations of NGC 346 were obtained through the offline queue between 2008 January 10 and 2009 December 23, with seeing values ranging from 0.″4 to 3.″1. Aperture differential photometry of NGC 346-013 and two nearby cluster members, MPG 781 (=Sk 80, NGC 346-001) and MPG 811, was performed using IRAF package APPHOT. Two moderately bright stars lie less than 3″ to the south-east of NGC 346-013 and, at the pixel scale of the FTS data, the three sources could not be separated by using aperture photometry alone. To overcome this a large 12-pixel aperture was used to include all three sources, making the assumption that the other two stars are non-variable and therefore any variability is solely due to the binary. The relative contribution of the target with respect to the other two stars was then measured by obtaining point spread function (PSF) photometry of one of the observations under excellent seeing, using IRAF/DAOPHOT. The two stars were found to contribute 34% of the light at phase $\phi = 0.7$.

3. Quantitative spectroscopic analysis of system

3.1. Atmospheric parameters

To determine effective temperatures (T_{eff}) and surface gravities (log g) for the orbital analysis, physical parameters for the secondary object were estimated using the non-LTE TLUSTY model atmosphere grid, discussed by Dufton et al. (2005) and used extensively in the analysis of B-type Magellanic Cloud stars from the FLAMES survey (e.g. Hunter et al. 2007; Trundle et al. 2007). Standard techniques were used to derive the physical parameters of the secondary. The effective temperature was estimated from the Si III/Si IV ionization equilibrium, and fits to the hydrogen lines were used to constrain the surface gravity. The Si III triplet at 4560 Å was used to estimate the microturbulence
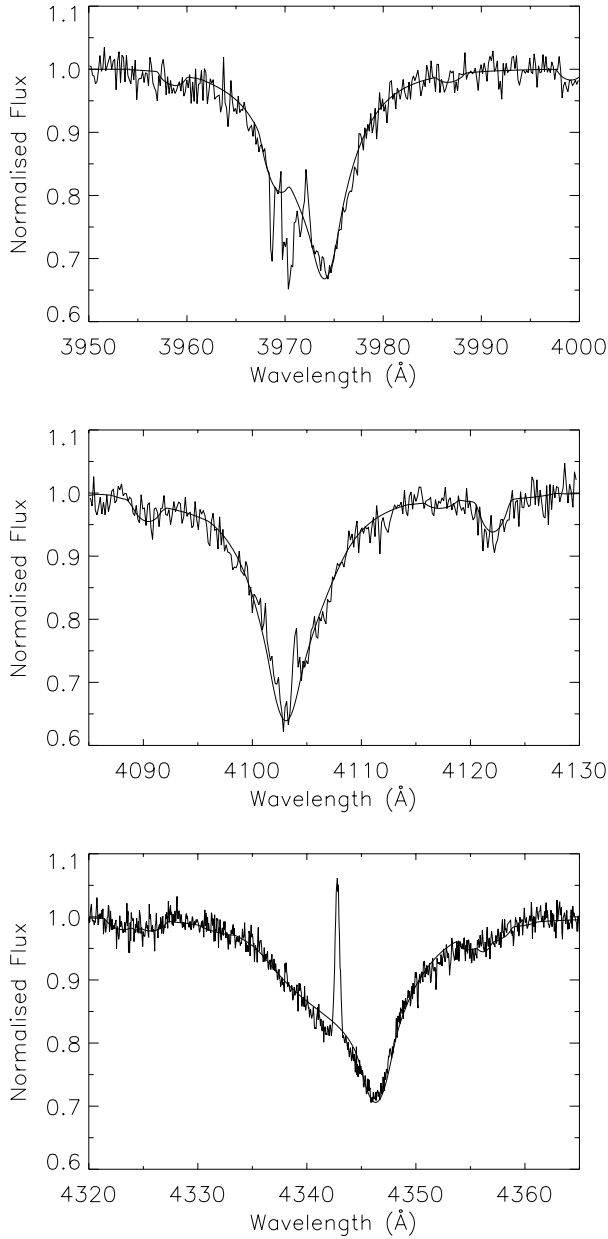
Fig. 3. Example fits to the metal absorption lines: (*top*) Si III triplet (*bottom*) N II 3995 line.

as the Hδ line where the primary and secondary are not well separated are shown in Fig. 2 and provide satisfactory fits in all cases. We derive $T_{\rm eff}$ = 24 500 K in reasonable agreement with the temperature scale from Trundle et al. (2007) for early B-type giants in the SMC. A microturbulence (ξ) of 4 km s^{-1} was estimated from the Si III triplet of lines. Conservative uncertainties on these results are $\Delta T_{\rm eff}$ = ±1500 K, $\Delta \log g$ = ±0.2, and $\Delta \xi$ = ±3 km s^{-1}.

Simultaneously to the analysis of the secondary object, the spectroscopic analysis of the primary object was carried out. The rotational velocity of the primary is much greater than the secondary (Sect. 3.2) which precludes the observation of the metal lines in its spectra. As such, the He II lines were utilised for the effective temperature estimate of the primary object by fitting the observed line with rotationally broadened model spectra over a range of parameters, with a best fit to the He II 4542 Å line found at an effective temperature of 34 500 K. The logarithmic gravity of the primary was calculated to be 3.90 dex from the fit to the hydrogen lines. Due to the weakness of the primary spectrum, errors are $\Delta T_{\rm eff}$ = ±3000 K and $\Delta \log g$ = ±0.3 respectively.

3.2. Rotational velocities

Similar methods to those discussed in Hunter et al. (2007) have again been used to estimate the rotational velocity of both the primary and secondary objects, viz. convolving the model spectra with rotationally-broadened profiles until a good fit to the observations is found. No metal lines are apparent from the primary, so we have used the He II line at 4686 Å to estimate a projected rotational velocity of 320 km s^{-1} for this object[7]. A

---

[7] This value is in excellent agreement with the fits to the He I lines used to measure the RV of the primary.

Fig. 2. Quality of model fits to the observed Hε, Hδ and Hγ lines (upper, middle and lower panels respectively) of both stars, with the B-star being 1.8 times brighter than the O-star. The absorption features in the blue flank of the Hε line are due to interstellar Ca II λ3968.

(see Hunter et al. 2007 for a detailed discussion). Deriving the atmospheric parameters is an iterative process and is further complicated by contamination of the spectra of the secondary by the O-type primary, and an estimate of the continuum contamination must therefore be included. The fitting of the hydrogen lines for the gravity estimate is dependent on the level of continuum contamination from the primary object, and a secondary 1.8 times brighter than the primary provides the best fit to the observed spectra (i.e. a continuum contamination of 35%). As the spectra of the primary and secondary objects are well separated in the HR02 and HR04 observations, the Hε and Hγ lines have been used to determine the surface gravity of the secondary object, with the best estimates being 3.40 dex and 3.50 dex from the two lines respectively. The individual fits to both these lines as well
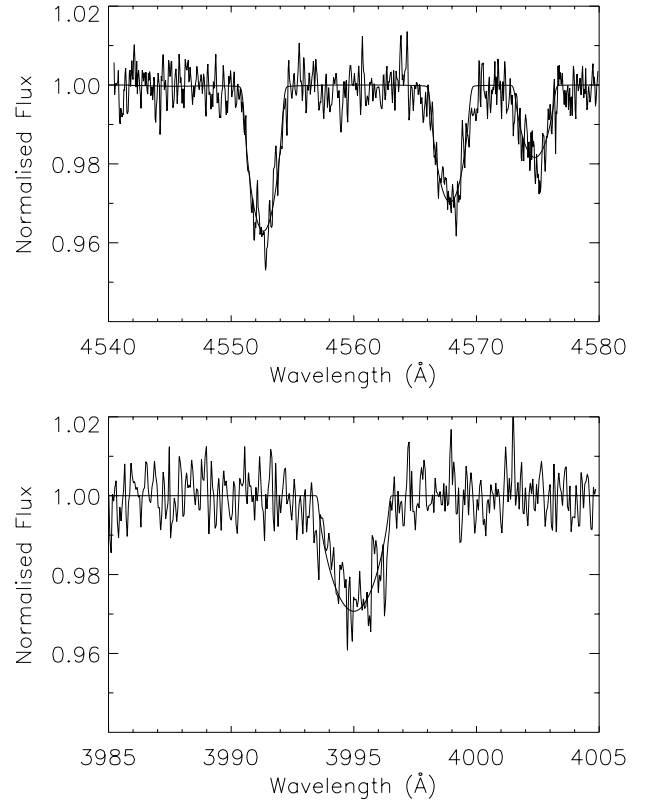
Table 3. Equivalent widths for the available metallic lines of the secondary.

Species	λ (Å)	$EW_{\text{meas.}}$ (mÅ)	$EW_{\text{corr.}}$ (mÅ)	$[X/H]$
N II	3995	62	98	7.54
O II	4069	89	129	8.19
O II	4072	65	99	8.34
O II	4076	75	117	8.35
O II	4591	51	80	8.21
O II	4596	48	75	8.23
O II	4662	42	66	8.04
Mg II	4481	53	34	6.68
Si III	4553	87	142	6.88
Si III	4568	69	108	6.85
Si III	4575	42	66	6.90
Si IV	4116	25	39	6.85

Notes. Abundances (where $[X/H] = \log(X/H)+12$) have been calculated by scaling the measured equivalent widths ($EW_{\text{meas.}}$) to give corrected widths ($EW_{\text{corr.}}$) assuming that the secondary is 1.8 times brighter than the primary.

Table 4. Atmospheric parameters for the secondary of NGC 346-013.

	NGC 346-013	SMC average
T_{eff} (K)	$24\,500 \pm 1\,500$	–
$\log g$	3.45 ± 0.2	–
v_{turb} (km s^{-1})	4 ± 3	–
[N/H]	7.54 ± 0.18	6.56
[O/H]	8.23 ± 0.23	8.02
[Mg/H]	6.68 ± 0.16	6.72
[Si/H]	6.87 ± 0.30	6.77

Notes. Mean abundances ($\log(X/H)+12$) and the uncertainties in these parameters are given. For comparison the mean SMC abundances from Hunter et al. (2007) are also included.

model profile at the estimated parameters discussed above was scaled to the same equivalent width as the observations in order to derive this value. However as the profile is rotationally dominated, errors in the underlying model spectrum should not be significant; nevertheless we adopt a conservative uncertainty of 30 km s^{-1}. Assuming a continuum contamination of 35% from the primary we derive a projected rotational velocity of 110 ± 10 km s^{-1} for the secondary object from the Si III triplet of lines.

3.3. Chemical abundances

Using the above parameters, chemical abundances for the secondary object have been determined (N, O, Mg and Si). The equivalent widths of the observed metal lines of the secondary have been measured and these measured equivalent widths are scaled to take into consideration the continuum contamination from the primary and then the abundances are estimated. The line-by-line equivalent widths and abundance estimates are given in Table 3 with the mean values being summarized in Table 4. Additionally we give the base-line chemical composition of the SMC as determined by Hunter et al. (2007) from the analysis of 14 early B-type objects. The O, Mg and Si abundances are in good agreement which further supports our derived continuum contamination parameter. Although the nitrogen abundance is ~1.0 dex enhanced over that of the SMC, Hunter et al. (2007, 2009) determined nitrogen abundances ranging from 6.5 dex to 7.6 dex and so the enhanced nitrogen abun-

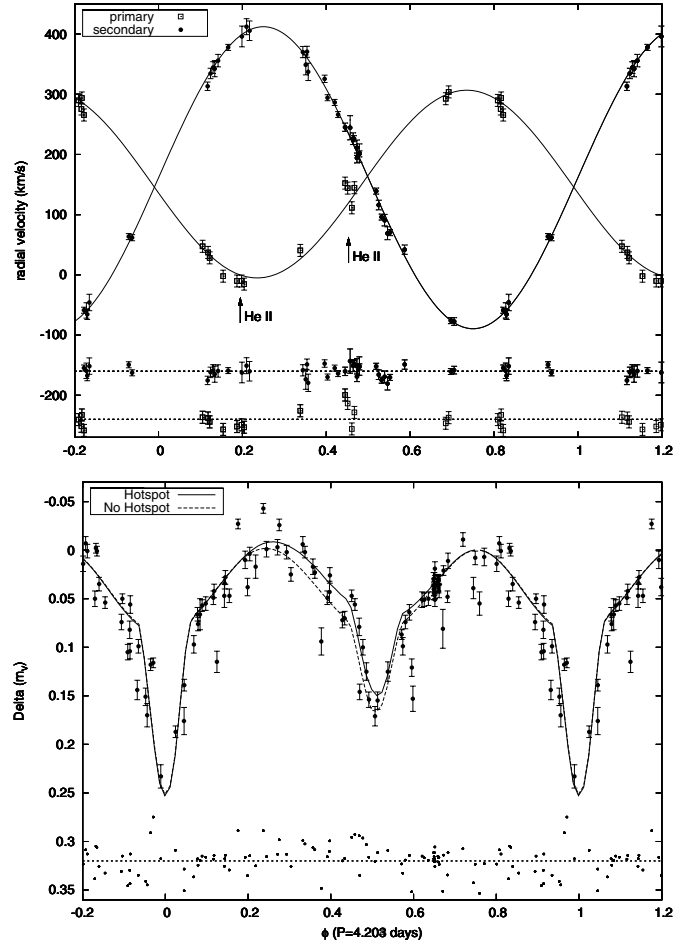**Fig. 4.** (*Top*) radial velocity curve for NGC 346-013. (*Bottom*) *Nightfall* fits to the *V*-band lightcurve. The solid and dashed lines show models with and without the hotspot discussed in the text; residuals are plotted for the no-hotspot model.

dance of the secondary in NGC 346-013 is not exceptional. In Fig. 3 we show model fits to example metallic lines.

The uncertainties given in Table 4 for the abundances include random uncertainties arising from measurement errors as well as the systematic uncertainties arising from errors in the atmospheric parameters, see Hunter et al. (2007) for a full discussion on the derivation of these uncertainties.

4. Orbital parameters

4.1. Radial velocity curve

An initial estimate of the orbital period was obtained using separate Lomb-Scargle periodograms of the radial velocity and photometric data, with the strongest peak in both datasets found at 0.238 cycles/day (corresponding to an orbital period of 4.202 days), with the 2008 FLAMES dataset therefore providing near-contiguous coverage of two complete orbits. Taking this initial estimate of the orbital period as a starting point, an iterative fit using the Levenberg-Marquardt algorithm was used to refine the period and determine the semi-amplitude and systemic velocity of the secondary; a non-zero eccentricity was allowed by the model, although all best fits were consistent with a circular orbit. The resulting solution is generally an excellent fit to the spectroscopic results (see the top panel

of Fig. 4), with a period 4.20381(12) days, superior conjunction at MJD 52 924.21553(66), semi-amplitude $K_2 = 250.1 \pm 2.8$ km s^{-1}, and a systemic velocity $\gamma_2 = 160.9 \pm 1.9$ km s^{-1} that is very close to the local gas velocity of 162.2 ± 1.8 km s^{-1} found from the strong nebular Hα line. Fixing the period and setting the phase as 180 degrees away from the secondary then yields a semi-amplitude and systemic velocity for the primary of $K_1 = 156.0 \pm 4.3$ km s^{-1} and $\gamma_1 = 150.8 \pm 3.3$ km s^{-1} respectively. We therefore find a mass ratio $q = M_2/M_1 = 0.62 \pm 0.02$,

$$M_1 \sin^3 i = \frac{(1+q)^2 P K_2^3}{2\pi G} = 18.0 \pm 0.8 \; M_\odot \tag{1}$$

and

$$M_2 \sin^3 i = 11.2 \pm 0.5 \; M_\odot. \tag{2}$$

4.2. Photometry

The *nightfall* code[8] was used to model the light curve of NGC 346-013. Following the analysis of Sect. 3.1, the temperature of the secondary was set at 24 500 K and a model atmosphere with $\log g = 3.5$ was used, while the primary was set at 34 500 K and $\log g = 4$, and the radius was set so that the B-type secondary was 1.8× more luminous than the O-star primary. Both temperatures were allowed to vary within the error range of the TLUSTY model. The eccentricity was initially set to zero, as implied by both the RV solution and the near-contact light curve, while the orbital period P and mass ratio q were fixed at the values derived in Sect. 4.1 and a "third light" contribution of 34% was set as discussed in Sect. 2.2. Detailed reflection was included in the model, and a linear limb-darkening law was assumed. Errors are internal to the model and do not include uncertainty in the "third light" contribution, although these do not strongly affect the derived inclination.

The model converges to an inclination of 78.3 ± 1.5 degrees, with a 11.2 $R_\odot$ secondary that has filled its Roche lobe and a 4.6 $R_\odot$ primary which is almost completely eclipsed at phase 0; we conservatively estimate errors on the radii of $\pm 0.6 \; R_\odot$ and $\pm 0.5 \; R_\odot$ respectively. In such a configuration the primary eclipse is therefore deeper than secondary eclipse, despite the smaller primary being intrinsically less luminous. The lightcurve fit favours a slightly lower temperature ratio than the TLUSTY model, with a 33 500 K primary and 25 000 K secondary, but poor photometric sampling of the primary eclipse leads to some uncertainty as to the primary temperature, and with errors of ± 2000 K and ± 1000 K respectively these values are consistent with the uncertainties of the fits to the FLAMES spectra. However, it was not possible to reproduce the clearly-asymmetric secondary eclipse well with the initial model, which also favoured a small degree of eccentricity ($e \sim 0.02 \pm 0.01$) to correctly reproduce the eclipse timing even though a non-circular orbit is inconsistent with the putative evolutionary state. The uneven secondary eclipse implies a non-uniform surface brightness, and this was modelled by including a "hotspot" on the trailing side (i.e. such that the luminosity of the secondary is systematically higher prior to eclipse entry, when the hotspot is visible, than after eclipse when the hotspot is not in the line of sight). When this effect was included, the resultant fit to the whole lightcurve was significantly improved, with a non-zero eccentricity no longer required to reproduce the eclipse timing. The best-fit hotspot has

---

[8] http://www.hs.uni-hamburg.de/DE/Ins/Per/Wichmann/Nightfall

Table 5. Summary of orbital and physical parameters of NGC 346-013 from the analysis in Sects. 4.1 and 4.2.

Parameter	Value	
T_0 (MJD)	52 924.21553(66)	
P (days)	4.20381(12)	
$q (= M_2/M_1)$	0.624 ± 0.019	
a ($R_\odot$)	34.4 ± 0.5	
i	$78.3° \pm 1.5$	
e	<0.02	
	Primary	Secondary
T_{TLUSTY} (K)	$34\,500 \pm 3000$	$24\,500 \pm 1500$
$T_{\text{NIGHTFALL}}$ (K)	$33\,500 \pm 2000$	$25\,000 \pm 1000$
$\log g$ (TLUSTY)	3.9 ± 0.3	3.45 ± 0.2
Filling factor	–	0.98 ± 0.02
R ($R_\odot$)	4.6 ± 0.5	11.2 ± 0.6
γ (km s^{-1})	150.8 ± 3.3	160.9 ± 1.9
K (km s^{-1})	156.0 ± 4.3	250.1 ± 2.8
$M \sin^3 i$ ($M_\odot$)	18.0 ± 0.8	11.2 ± 0.5
M ($M_\odot$)	19.1 ± 1.0	11.9 ± 0.6

a temperature ratio of ~1.5 ($T \sim 38$ kK) and a longitude $-30°$ that imply that the hotspot is not caused by irradiation by the hotter primary, and instead reflects a region where the primary wind interacts with the photosphere of the secondary[9]. Fits to the light curve both with and without the inclusion of a hotspot are shown in the bottom panel of Fig. 4, with parameters listed in Table 5. Considerable scatter is present in the photometry, with some data points between phases ~0.75 and ~0.95 appearing to favour the "no-hotspot" model. These data were obtained over a two-year baseline, and we therefore speculate that variability may be present in this feature, while the true interaction is undoubtedly more complex than the simple hotspot considered here. However, we note that omission of the hotspot does not significantly affect either the derived inclination or the conclusion that the secondary has filled its Roche lobe.

4.3. Orbital parameters

Combining the radial velocity and photometric models, we find masses for the two components of $19.1 \pm 1.0 \; M_\odot$ and $11.9 \pm 0.6 \; M_\odot$ respectively, with the latter value consistent with the ~B1 spectral type of the secondary, e.g. the evolutionary masses from Hunter et al. (2007) and Trundle et al. (2007). From the orbital parameters we find a separation of 34.4 $R_\odot$, with a circular orbit ($e < 0.02$) as expected for a Roche-lobe filling system. Synchronous rotation would imply $v \sin i$ of 132 km s^{-1}, somewhat faster than the $v \sin i$ of 110 km s^{-1} found from the spectral line widths of the secondary; we return to this issue in Sect. 5.1. Taking the photometric radius of $11.2 \pm 0.6 \; R_\odot$ and secondary mass of $11.9 \pm 0.6 \; M_\odot$ gives $\log g = 3.43$, in excellent agreement with the spectroscopic value of $\log g = 3.45$ determined in Sect. 3. The primary radius $4.6 \pm 0.5 \; R_\odot$ implies $\log g \sim 4.4 \pm 0.1$, somewhat higher than inferred from the model fit to the hydrogen lines[10], while the derived radius appears rather low compared to galactic O9 dwarfs (cf. the list of detached O binaries in Gies 2003, or V3903 Sag., a detached, short-period

---

[9] This is very similar to the effect found in the 6.6-day contact binary Cyg OB2#5 by Linder et al. (2009).

[10] This discrepancy may reflect the effects of rapid rotation and a lower effective equatorial surface gravity on the hydrogen line profiles.

O7+O9 binary in which the secondary has a near-identical mass and temperature to the primary in NGC 346-013 but a radius ~25% higher; Vaz et al. 1997). However, the derived values are broadly consistent with a 20 $M_\odot$ model at SMC metallicity with a zero-age main sequence radius of 5.2 $R_\odot$ at T_{eff} = 36 000 K and $\log g$ = 4.3 (Brott et al. 2011), and the photometric and model atmosphere values are in acceptable agreement given the limitations of the photometric dataset and the paucity of spectral features from the O-star.

4.4. Alternative lightcurve model

If the radius of the primary is not constrained to ensure the brightness ratio implied by the model fits to the hydrogen lines, we find an alternative lightcurve fit at somewhat lower inclination (71° ± 2) in which the general properties of the B-type secondary are broadly unchanged but the O-type primary has a radius 12 ± 1 $R_\odot$ and Roche-lobe filling factor ~0.8 ± 0.1 that makes it slightly larger than its companion and consequently significantly *more* luminous. Revised masses for the system then become 21.3 ± 1.3 $M_\odot$ and 13.3 ± 0.8 $M_\odot$ respectively. In this configuration neither component is deeply eclipsed, while inclusion of "hotspots" on the B-type star is again required to recreate the profile of the secondary eclipse. However, TLUSTY model fits to the Balmer series lines discussed in Sect. 3.1 are strongly inconsistent with a more luminous primary, and it was not possible to achieve an acceptable fit to the FLAMES spectra with this alternative model. Consequently we do not favour this solution, but additional spectroscopic and photometric observations will be required to conclusively resolve this possible discrepancy.

5. Discussion

5.1. Evolutionary state

Few clues to the nature of the primary are found in our spectra, with the majority of features within the FLAMES coverage originating in the ~B1 secondary. Modelling suggests a temperature of ~34.5kK and an ~O9–9.5 V spectral type for the primary, while the high rotational velocity of ~320 km s^{-1} derived from the broad He II lines (see Sect. 3.2) implies that it has been "spun up" by mass transferred from the secondary, as tidal effects in close binary systems are otherwise expected to lead to synchronization of rotation. The secondary appears to be rotating somewhat slower than expected for a synchronized system, consistent with a predicted spin-down of the mass donor during mass transfer (Langer 1998; Langer et al. 2003), and has almost filled its Roche lobe, implying that despite its *current* lower mass it is in a more advanced evolutionary state. The primary appears somewhat underluminous for its mass (see Fig. 5), consistent with a mass-gainer that has not rejuvenated completely (Braun & Langer 1995); significant helium enrichment indicative of a more evolved state would place it close to the Wolf-Rayet phase, with an implied luminosity of $\log(L/L_\odot) > 5.5$ inconsistent with our observations. We note that the system does not feature in
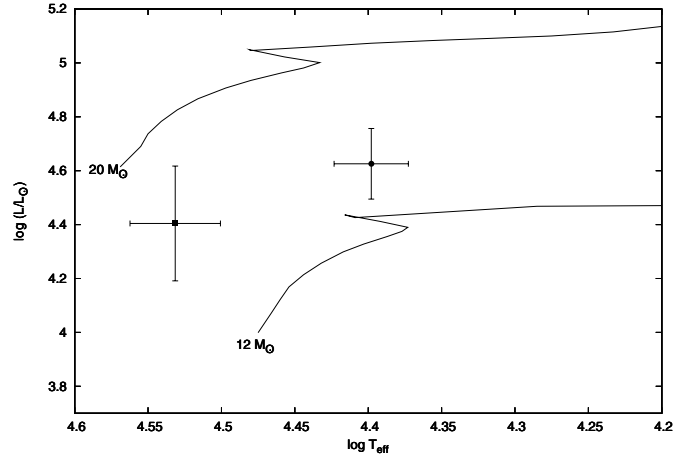

Fig. 5. Location of the primary and secondary relative to illustrative SMC evolutionary tracks from Maeder & Meynet (2001) appropriate for the *current* masses of the two components.

the X-ray catalogue from *Chandra* observations of the NGC 346 region by Nazé et al. (2003), but the expected X-ray luminosities of $\lesssim 10^{32}$ erg s^{-1} characteristic of individual OB stars (Clark et al. 2008) are too low for detection[11] unless X-ray emission is significantly enhanced via wind interaction.

At first sight two stars of near-equal initial mass, i.e. M_{ini} ~ 16 + 15 $M_\odot$, and an orbital period of a few days would appear a simple model of the precursor to the current system. If the initial period is very short ($P \lesssim 2.5$ days) such a configuration may reach contact and merge while both stars are still on the main sequence (Wellstein et al. 2001; Petrovic et al. 2005), but for slightly longer periods the system will evolve via quasi-conservative case A mass transfer as the initially more massive star overflows its Roche lobe, potentially allowing the exchange of the ~4 $M_\odot$ needed to reach the current 19 + 12 $M_\odot$ mass ratio while "spinning up" the mass gainer to rapid rotation. However, in such a scenario mass transfer would not halt at this point, but would continue at very high rates ($\gtrsim 10^{-4}$ $M_\odot$ yr^{-1}; Wellstein et al. 2001) until most of the hydrogen envelope of the mass donor is lost: the eclipsing binary RY Scuti appears to be possibly the only known example of this process in action, with ongoing mass transfer from an 8 $M_\odot$ primary to a 30 $M_\odot$ companion embedded in a dense accretion disk (Smith et al. 2011). The current mass ratio of NGC 346-013 would therefore place it in the middle of fast case A transfer, but the expected duration of this phase is so short (~10^4 years) that direct observation is unlikely, while the extensive circumstellar material (and possibly B[e] star morphology) indicative of rapid mass transfer is not observed.

At the end of the rapid phase of case A transfer, "slow" transfer commences, lasting for ~1 Myr at rates ~10^{-7} $M_\odot$ yr^{-1} (Wellstein et al. 2001; Langer et al. 2003). An initial 16 + 15 $M_\odot$ system would start the slow phase with an overluminous low-mass donor and a rapidly-rotating accretor with M ~ 25 $M_\odot$ (Wellstein et al. 2001; Langer et al. 2003), but a higher mass initial configuration provides a much better match: taking model 13 of Wellstein & Langer (1999) as a template, a 22 + 18 $M_\odot$ system in an inital three-day orbit will exit the fast phase of mass transfer with an 11.5 $M_\odot$ mass donor that still fills its Roche lobe, very similar to the B-type star in NGC 346-013. The model is not perfect, as at the end of the fast phase of mass transfer both

---

[11] The faintest sources in Nazé et al. (2003) have fluxes of ~6 × 10^{32} erg s^{-1}, assuming a distance of 59 kpc for the SMC.

the orbital period of 7.3 days and the 28.5 $M_\odot$ mass-gainer are again inconsistent with the current state of NGC 346-013, but the model was computed assuming fully conservative mass transfer with no loss of mass or angular momentum from the system. However, models including rotation indicate that mass transfer may be significantly *non*-conservative, with only a fraction of the transferred material retained by the accretor while the remainder is ejected from the system (Petrovic et al. 2005). Assuming an efficiency $\beta \sim 50\%$ and a slightly greater initial mass ratio of $\sim 22 + 15\ M_\odot$, at the end of the fast phase system we would again observe an 11.5 $M_\odot$ mass donor, but the accretor would have only increased in mass to $\sim 20\ M_\odot$, in good agreement with our observations, while the loss of angular momentum from the system might be sufficient to restrict the increase in orbital period. The B-type star would be expected to have nitrogen enhanced by up to 1 dex as CNO-processed material is exposed by the loss of the hydrogen envelope (Petrovic et al. 2005; Langer et al. 2008), consistent with the high (but not exceptional) nitrogen abundance found in Sect. 3.3.

Such a scenario requires confirmation from binary evolutionary models tailored to match the parameters of NGC 346-013, but represents an encouraging match to the observations of the system. Tidal effects are expected to slow the rotation of the mass gainer within a few 10^5 years (Petrovic et al. 2005), with the still-rapid rotation of the primary therefore suggesting that fast transfer has ended relatively recently. Within $\sim 10^6$ years the system will return to synchronous rotation, while slow case A transfer will finish when core hydrogen burning ends in the mass donor. A second phase of rapid case AB transfer then commences with the onset of shell burning, spinning up the O-type star, still on the main sequence, back to near-critical rotation (Langer et al. 2003). During this phase the mass donor will lose its remaining hydrogen envelope to leave a helium core, while the orbital period expands greatly (Wellstein et al. 2001), leaving a rapidly rotating $\sim 20-25\ M_\odot$ OB (super)giant that appears as an apparently-single star, with the extreme mass ratio and increasingly low luminosity of the mass donor making detection challenging. The initially more massive star will ultimately end its life as a type Ib/c supernova, forming a neutron star due to the reduced core mass resulting from loss of the hydrogen envelope (Petrovic et al. 2005) and the early termination of shell hydrogen burning (Brown et al. 2001). In contrast, the spun-up mass gainer may then evolve under chemically homogeneous evolution, returning to critical rotation at the end of core hydrogen burning and ultimately forming a rapidly-rotating Wolf-Rayet star that may represent a future γ-ray burst progenitor (cf. Cantiello et al. 2007).

5.2. NGC 346-013 in the context of the SMC binary population

The advent of large multi-object spectrographs has allowed the efficient follow-up of eclipsing binaries identified in large photometric surveys (e.g. OGLE-2; Udalski et al. 1997), and accurate parameters are now available for significant numbers of SMC binary systems (e.g. Harries et al. 2003; Hilditch et al. 2005; and North et al. 2010), while modelling of the Hilditch et al. (2005) dataset has been carried out by de Mink et al. (2007). In the context of these samples the 19.1 ± 1.0 and $11.9 \pm 0.6\ M_\odot$ components of NGC 346-013 are unexceptional, with several more massive systems listed by Hilditch et al. (2005), who also identify some 28 systems as being in a post-Roche-lobe overflow state consistent with the quasi-conservative models of Wellstein et al. (2001). However, in these samples objects near $\sim 20\ M_\odot$

have luminosities 0.1–0.5 dex higher than the O-type primary of NGC 346-013, while the 320 km s^{-1} projected rotational velocity is also substantially higher than any object listed by North et al. (2010), supporting the conclusion that we are observing NGC 346-013 in an unusual evolutionary state.

OGLE 5202153 ($P = 4.61$d, $20 + 13\ M_\odot$; Harries et al. 2003) appears very similar to NGC 346-013, with an O9.5 primary displaying He II absorption that is absent in the spectrum of the Roche-lobe filling B0.5 III secondary. The light curve is also asymmetric, although in this case the luminosities of the two components are similar, a result of a larger primary radius than we infer here. de Mink et al. (2007) model the evolution of this system, and find non-conservative models ($\beta = 0.5$) give a better fit than fully-conservative mass transfer. Additional parameters such as chemical abundances and the projected rotational velocity of the primary that would confirm the similarity of NGC 346-013 and OGLE 5202153 are not known. Two further systems, OGLE 5300549 ($P_{\rm orb} = 1.33$d, $25 + 17\ M_\odot$; Hilditch et al. 2005) and OGLE 9163232 (=Hodge 53-47, $P_{\rm orb} = 2.21$d, $26 + 16\ M_\odot$; Harries et al. 2003; Morrell et al. 2003) are identified by Hilditch et al. (2005) as objects that may have recently exited the fast phase of mass transfer. Morrell et al. (2003) suggest that the O6 V and O4–5 III(f) components of OGLE 9163232 have undergone significant mass transfer, although the current 2.2-day orbital period would require a particularly compact initial configuration, and the system may ultimately merge as the O6 V mass gainer ends core hydrogen burning, fills its Roche lobe, and begins reverse mass transfer while the mass donor is still on the main sequence (Wellstein et al. 2001; see also de Mink et al. 2007). OGLE 5300549 has a B0 primary that, like NGC 346-013, also seems somewhat underluminous for its mass, while the system has the largest temperature ratio in the sample of Hilditch et al. (2005). In this case the orbital period is so short that the rotational mixing pathway of de Mink et al. (2009) is important, and identification as a post mass-transfer system may be uncertain.

5.3. Evolutionary implications for NGC 346

The systemic velocity of NGC 346-013 (~ 155 km s^{-1}) is comparable with the radial velocities of non-binary members of NGC 346 (e.g. Evans et al. 2006), while the location 2′.34 (equivalent to 41 pc at the distance of the SMC) from the O4 III(f) star MPG 435[12] in the central core (Massey et al. 1989) places it well within the $\sim 7'$ ionized region of NGC 346 (Relaño et al. 2002)[13]. NGC 346-013 therefore appears to be a true member of the cluster and does not appear to have been ejected.

Sabbi et al. (2007) report extensive subclustering in NGC 346, with NGC 346-013 apparently associated with SC-16, a subcluster with radius 1.6pc that likely pre-dates the formation of the main NGC 346 cluster. An age of 15 ± 2.5 Myr is reported for SC-16 by Sabbi et al. (2007), consistent with independent determinations of 5–15 Myr (Hennekemper et al. 2008) and 12.5–18 Myr (Cignoni et al. 2010), but notably discrepant with ages of 3 ± 1 Myr for the subclusters that trace the major epoch of star formation in NGC 346. However, ages of ≥ 10 Myr are incompatible with NGC 346-013 being a bona fide member of SC-16, as even with minimum progenitor masses the system would start to

---

[12] $\alpha = 00{:}59{:}04.49$, $\delta = -72{:}10{:}24.68$ (J2000).

[13] The radial distance from the centre of the cluster was given by Evans et al. (2006) as 1.89′; this distance was calculated taking coordinates for the centre of the cluster from SIMBAD (http://simbad.u-strasbg.fr).

interact at an intermediate age ($\sim$8 Myr; Langer et al. 2008) and comparison with SMC evolutionary tracks (Maeder & Meynet 2001) shows that core hydrogen burning would have ended at $\sim$10 Myr, while at the ages reported by Sabbi et al. (2007) and Cignoni et al. (2010) core helium burning would also have ended[14]. Higher progenitor masses would imply earlier interaction, and it therefore seems possible that NGC 346-013 represents a chance association with SC-16, and is more likely to have an age compatible with the main burst of star formation in NGC 346. However, a young age for SC-16 might nevertheless be consistent with NGC 346-013 being a member, and any conclusive determination of the likely age and formation scenario for NGC 346-013 and its consequent implications for the star formation history of NGC 346 must also await tailored modelling with binary evolution codes.

6. Conclusions and future work

We find current masses of 19.1 $\pm$ 1.0 $M_\odot$ and 11.9 $\pm$ 0.6 $M_\odot$ for the O- and B-type components of NGC 346-013 respectively, with comparison with tailored non-LTE model atmosphere spectra favouring a more luminous B-type star and consequently a compact O-type primary of 4.6 $\pm$ 0.5 $R_\odot$. Simple conservative mass transfer in an initial 16+15 $M_\odot$ system appears unlikely, and we suggest that the system began life as a $\sim$22+15 $M_\odot$ binary, with the current B-type secondary initially the more massive star, and has recently exited a phase of rapid, non-conservative mass transfer that has spun the current primary up to high rotation. This scenario suggests an age of $\lesssim$6 Myr consistent with the recent burst of star formation within NGC 346. Within $\sim$1–2$\times$10^6 years the system will undergo a second phase of fast case AB mass transfer to form a low-mass helium star + OB (super)giant binary with a period of months. The initially more massive star will ultimately form a neutron star and, if the system is not disrupted by a supernova "kick", a long-period neutron star + OB supergiant high-mass X-ray binary, while the mass gainer may subsequently evolve at high rotation and may be a possible γ-ray burst progenitor.

Further optical observations will allow a search for evidence of other spectral features originating from the primary, in order to better constrain its nature; in particular ultra-violet data could offer insight, as the O-type star would be expected to dominate the flux in that region. High quality photometric data would also resolve the uncertainty as to the radius of the primary, and would test the robustness of the orbital parameters presented here. However, despite this uncertainty the general properties of the system are well constrained, and it therefore represents an excellent candidate for tailored modelling with binary evolution codes.

References

Blecha, A., North, P., Royer, F., & Simond, G. 2003, GIRAFFE BLDR Software – Reference Manual, 1st edn. (Observatoire de Genève)
Braun, H., & Langer, N. 1995, A&A, 297, 483
Brott, I., de Mink, S. E., Cantiello, M., et al. 2011, A&A, 530, A115
Brown, G. E., Heger, A., Langer, N., et al. 2001, NewA, 6, 457
Cantiello, M., Yoon, S.-C., Langer, N., & Livio, M. 2007, A&A, 456, 29
Cignoni, M., Tosi, M., Sabbi, E., et al. 2010, ApJ, 712, 63
Cignoni, M., Tosi, M., Sabbi, E., Nota, A., & Gallagher, J. S. 2011, AJ, 141, 31
Clark, J. S., Goodwin, S. P., Crowther, P. A., et al. 2002, A&A, 392, 909
Clark, J. S., Muno, M. P., Negueruela, I., et al. 2008, A&A, 477, 147
Clark, J. S., Ritchie, B. W., Negueruela, I., et al. 2011, A&A, 531, A28
Dufton, P. L., Ryans, R. S. I., Trundle, C., et al. 2005, A&A, 434, 1125
Eldridge, J. J., Izzard, R. G., & Tout, C. A. 2008, MNRAS, 384, 1109
Evans, C. J., Smartt, S. J., Lee, J.-K., et al. 2005, A&A, 437, 467
Evans, C. J., Lennon, D. J., Smartt, S. J., & Trundle, C. 2006, A&A, 456, 623
Gies, D. R. 2003, in A Massive Star Odyssey: From Main Sequence to Supernova, ed. K. A. van der Hucht, A. Herrero, & C. Esteban (San Fransisco: ASP), IAU Symp., 212, 91
Gouliermis, D. A., Bestenlehner, J. M., Brandner, W., & Henning, T. 2010, A&A, 515, A56
Harries, T. J., Hilditch, R. W., & Howarth, I. D. 2003, MNRAS, 339, 157
Henize, K. G. 1956, ApJS, 2, 315
Hennekemper, E., Gouliermis, D. A., Henning, T., Brandner, W., & Dolphin, A. E. 2008, ApJ, 672, 914
Hilditch, R. W., Howarth, I. D., & Harries, T. J. 2005, MNRAS, 357, 304
Howarth, I. D., Murray, J., Mills, D., & Berry, D. S. 2003, in Starlink User Note 50.24, Rutherford Appleton Laboratory
Hubeny, I., & Lanz, T. 1995, ApJ, 439, 875
Hunter, I., Dufton, P. L., Smartt, S. J., et al. 2007, A&A, 466, 277
Hunter, I., Brott, I., Langer, N., et al. 2009, A&A, 496, 841
Kaper, L., van der Meer, A., & Najarro, F. 2006, A&A, 457, 595
Langer, N. 1998, A&A, 329, 551
Langer, N., Wellstein, S., & Petrovic, J. 2003, in A Massive Star Odyssey, from Main Sequence to Supernova, ed. K. A. van der Hucht, A. Herrero, & C. Esteban (San Fransisco: Astron. Soc. Pac.), IAU Symp. 212, 275
Langer, N., Cantiello, M., Yoon, S.-C., et al. 2008, in Massive Stars as Cosmic Engines, ed. F. Bresolin, P. A. Crowther, & J. Puls (Cambridge: Cambridge Univ. Press), IAU Symp., 250, 167
Linder, N., Rauw, G., Manfroid, J., et al. 2009, 495, 231
Maeder, A., & Meynet, G. 2001, A&A, 373, 555
Massey, P., Parker, J. W., & Garmany, C. D. 1989, AJ, 98, 1305
de Mink, S. E., Pols, O. R., & Hilditch, R. W. 2007, A&A, 467, 1181
de Mink, S. E., Cantiello, M., Langer, N., et al. 2009, A&A, 497, 243
Morrell, N., Ostrov, P., Massey, P., & Gamen, R. 2003, 341, 583
North, P., Gauderon, R., Barblan, F., & Royer, F. 2010, A&A, 520, A74
Nazé, Y., Hartwell, J. M., Stevens, I. R., et al. 2003, ApJ, 586, 983
Petrovic, J., Langer, N., & van der Hucht, K. A. 2005, A&A, 435, 1013
Relaño, M., Peimbert, M., & Beckman, J. 2002, ApJ, 564, 704
Ritchie, B. W., Clark, J. S., Negueruela, I., & Langer, N. 2010, A&A, 520, A48
Sabbi, E., Sirianni, M., Nota, A., et al. 2007, AJ, 133, 44
Simon, J. D., Bolatto, A. D., Whitney, B. A., et al. 2007, ApJ, 669, 327
Smith, N., Gehrz, R. D., Campbell, R. et al. 2011, MNRAS, 418, 1959
Trundle, C., Dufton, P. L., Hunter, I., et al. 2007, A&A, 471, 625
Udalski, A., Kubiak, M., & Szymanski, M. 1997, Acta Astron., 47, 319
Vaz, L. P. R., Cunha, N. C. S., Vieira, E. F., & Myrrha, M. L. M. 1997, A&A, 327, 1094
Walborn, N. R., Lennon, D. J., Heap, S. R., et al. 2000, PASP, 112, 124
Wellstein, S., & Langer, N. 1999, A&A, 350, 148
Wellstein, S., Langer, N., & Braun, H. 2001, A&A, 369, 939
Woosley, S. E., & Heger, A. 2006, ApJ, 637, 914

---

[14] While the inclusion of rotation in the evolutionary tracks results in core hydrogen burning ending slightly later, the expectation that a short-period binary will reach synchronous rotation implies that the tracks with rapid rotation do not apply.